Pressurized internal lenticular cracks at healed mica interfaces

K-T. Wan,[a] R. G. Horn,[b] S. Courmont,[c] and B. R. Lawn
Materials Science and Engineering Laboratory, National Institute of Standards and Technology, Gaithersburg, Maryland 20899

(Received 28 September 1992; accepted 8 January 1993)

The equilibrium states of internal penny cracks at interfaces in thin-sheet bodies are investigated. Consideration is given to cracks held open by a center-loading force from an entrapped particle in combination with a uniform pressure from a fixed mass of entrapped gas. A fracture mechanics analysis indicates that under these conditions the cracks are stable, but are amenable to growth from an enhancement in net pressure (increase in internal pressure or decrease in external pressure) or effective particle size. Essential details of the theory are confirmed by experiments on lenticular cracks at healed interfaces in muscovite mica. The results are pertinent to flaw responses in brittle ceramic systems where structural integrity is an issue.

I. INTRODUCTION

It has long been recognized that inherent crack-like flaws from material fabrication processes can have a profound influence on the performance of structural ceramics. The most immediate manifestation of such flaws is a degradation in bulk strength.[1,2] In the special case of *internal* cracks parallel and adjacent to a free surface, the attendant fracture mechanics bear strongly on such issues as coating/substrate integrity,[3] subsurface damage and associated wear in tribological applications,[4] and internal flaw growth from particle- (electron or proton) and photon- (laser) radiation-induced damage.[5–7] The study of near-surface internal cracks is, therefore, of potential interest in the strength characterization of brittle materials.

In the present paper we study the mechanics and thermodynamics of internal cracks formed at healed interfaces in muscovite mica sheets. Results of earlier observations on this system[8,9] have demonstrated the advantages of mica as a model material for such a study. On recontacting thin, freshly cleaved, atomically smooth mica flakes, axisymmetrical lenticular cracks can be formed at the adhered interface, even with the mica sheets in mutual angular misorientation. These cracks are primarily held open by spurious mica flakes wedged between the opposing walls. Additionally, air trapped at the interface during closure can cause an excess pressure within the crack cavity.[9] In extreme cases, as we shall see, such a pressure buildup may constitute the *only* opening force keeping the crack open. The radii of the cracks formed are generally more than an order of magnitude greater than the thickness of an individual mica sheet, satisfying a necessary condition for the application of simple thin-plate elasticity theory to fracture mechanics problems.[10] Moreover, whereas the mismatch dilation of the healed interface is not sufficient to allow major constituents of the air within the cavity to diffuse out over any significant period of time, the same is not true of the smaller water molecules; by increasing or decreasing the external humidity, the cracks expand or contract, typically over a period of several hours, as water molecules ingress or egress to equilibrate the internal and external humidity.[9] This means that, notwithstanding any differences in internal gas pressure from crack to crack, the interface energy is spatially invariant, governed by the ambient humidity.[11,12] Hence we have a well-defined system, with predetermined fracture energy, for fracture mechanics analysis.

We begin our study with theoretical derivations of the crack profiles and energy balance relations for internally supported penny cracks. Consideration is given first to cracks with just center-particle support and with just gas-pressure support. Then the case of combined support is treated. It is assumed that variations in internal pressure and volume are constrained by the ideal gas law. Radial profile measurements on artificially formed cracks in healed mica sheets, at ambient and reduced external pressure, are used to illustrate the main theoretical predictions. It is shown that internal pressure can be an important, even dominant, factor in determining the nature, size, and stability of internal cracks in brittle materials.

[a]Doctoral Student, Department of Physics and Astronomy, University of Maryland, College Park, Maryland 20742.
[b]Now at Schools of Applied Physics and Chemical Technology, University of South Australia, The Levels, South Australia 5095, Australia.
[c]Work done while on leave from Ecole Superieure de Physique et de Chimie Industrielles de la Ville de Paris, F-75231 Paris.

II. MECHANICS AND THERMODYNAMICS OF CENTER-LOADED PRESSURIZED LENTICULAR CRACK

In this section we develop a fracture mechanics description for internal lenticular cracks embedded in a resealed interface. Our approach is to compute the mechanical energy U_M in the lenticular-crack plates as the work to displace these walls by a center-particle force and a uniform internal pressure. To do this we treat the crack walls as elastic half-plates clamped into an infinite rigid plate at their circumference. Our analysis embodies the following assumptions: (i) the crack radius is large compared to the sheet thickness, so that the thin-plate theory is valid; (ii) the two opposing crack walls are of equal thickness, and are of the same material, so that mode II components are absent; (iii) the normal crack-wall displacements are small compared to the sheet half-thicknesses so that membrane stresses[10] may be ignored. Then we compute the Griffith–Irwin mechanical-release-rate $G = -dU_M/dC$ with respect to crack area $C = \pi c^2$, with c the crack radius. The condition $G = W$ for crack equilibrium is governed by the Dupré work of adhesion, $W = 2\gamma_{BE}$, with $2\gamma_{BE}$ the interface energy for the body B in the presence of the environment E.[2,12,13] Again, for our specific system of rehealed/misoriented mica in controlled ambient (Sec. III), the interface energy is to be regarded as a predeterminable, invariant quantity.

A. Crack with center-point fixed-displacement loading

Consider the case where a lenticular crack of radius c is supported only by a rigid particle of dimension $2h$ (Fig. 1) trapped in the interface without any excess internal pressure. Each crack wall is subject to fixed central-opening displacements h, corresponding to central forces P [Fig. 1(a)]. From thin-plate elasticity, the wall displacement at a radial distance r is given by[10]

$$u_P(r) = u_P^0[1 - (r/c)^2 - 2(r/c)^2 \ln(c/r)], \quad 0 \leq r \leq c. \tag{1}$$

The central displacement, $u_P(0) = u_P^0 = h = \text{constant}$, is given by[10]

$$u_P^0 = h = 2Pc^2/4\pi E'd^3, \tag{2}$$

where d is the wall thickness, and $E' = E/(1 - \nu^2)$ with E Young's modulus and ν Poisson's ratio. The volume of the crack can be immediately calculated by integrating $u_P(r)$ over the crack plane:

$$V_P = \frac{1}{2}\pi hc^2. \tag{3}$$

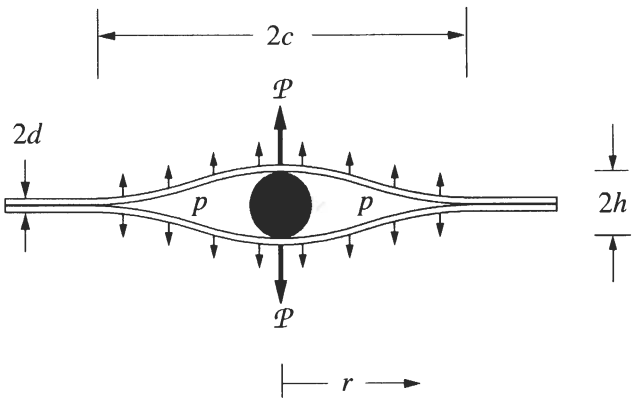

FIG. 1. Lenticular crack of radius c in a thin beam specimen of half-thickness d, supported by combined central point force P from a particle of radius h and uniform pressure p from internally trapped gas.

The mechanical energy U_M, and thence G, can be computed by integrating the force P at $r = 0$ through the displacement h for the two plates:

$$G_P(c, P) = 3P^2/4\pi^2 E'd^3. \tag{4}$$

Note that since P varies inversely with c at constant h in Eq. (2), G also varies inversely with c, so the crack is inherently *stable* in this loading. Combining Eqs. (2) and (4), we obtain the equilibrium crack size at $G = W$ in terms of h,

$$c = (4E'd^3h^2/3W)^{1/4}. \tag{5}$$

B. Crack with internal uniform pressure loading

In this subsection, we consider fully pressurized internal lenticular cracks held open only by a uniform excess internal pressure,

$$p = p_i - p_e, \tag{6}$$

with p_i and p_e the internal and external pressures. From thin-plate elasticity theory,[10]

$$u_p(r) = u_p^0[1 - (r/c)^2]^2, \quad 0 \leq r \leq c, \tag{7}$$

with central displacements $u_P(0) = u_p^0$ related to P by[10]

$$u_p^0 = 3pc^4/16E'd^3. \tag{8}$$

The crack volume is again obtained by integration over the crack plane:

$$V_p = \pi pc^6/8E'd^3. \tag{9}$$

The system mechanical energy is determined by integrating the uniform internal stresses through the outward displacements over the entire crack surfaces, from which we obtain

$$G_p(c, p) = 3p^2c^4/16E'd^3. \tag{10}$$

Note that G increases with p, so the crack would be *unstable* if p were to remain constant. However, as we shall see later, p itself tends to diminish with increasing c, such that the crack actually becomes *stable*. At equilibrium, $G = W$, we have

$$c = (16E'd^3W/3p^2)^{1/4}. \quad (11)$$

C. Combined center-point and uniform pressure loading

Now let us consider the cooperative effect of a central point force P and an excess uniform internal pressure p. The crack profile is given by the superposition of Eqs. (1) and (2) with Eqs. (7) and (8), $u_{P+p}(r) = u_P(r) + u_p(r)$, subject to the constraint $u_{P+p}(0) = u_0 = h$ = constant, i.e.,

$$u_0 = (3c^2/4E'd^3)(P/\pi + pc^2/4) = h, \quad (12)$$

yielding

$$u_{P+p}(r) = h[1 - (r/c)^2 - 2(r/c)^2 \ln(c/r)] - (3pc^4/16E'd^3)(r/c)^2[1 - (r/c)^2 - 2 \ln(c/r)], \quad 0 \leq r \leq c. \quad (13)$$

The crack volume is once more determined by integration over the crack plane:

$$V_{P+p} = \frac{1}{2}\pi c^2(h + pc^4/16E'd^3). \quad (14)$$

To find the equilibrium configuration for the crack with superposed loadings, we note that it is the stress-intensity factor $K = (GE')^{1/2}$ and not the energy-release rate G itself that is additive for a given fracture mode,[2] i.e.,

$$K_{P+p} = K_P + K_p \quad (15)$$

with K_P determined from Eq. (4) and K_p from Eq. (10). The net mechanical-energy-release rate is then given by $G_{P+p} = (K_P + K_p)^2/E'$, i.e.,

$$G_{P+p}(c, p, P) = (3/4E'd^3)[P/\pi + pc^2/2]^2 = \frac{4}{3}E'd^3[h/c^2 + 3pc^2/16E'd^3]^2. \quad (16)$$

The first term in the square bracket is due to the central point force and the second to the excess internal pressure. Note that Eq. (16) reduces to Eq. (4) for $p = 0$ and Eq. (10) for $P = 0$. At $G = W$, Eq. (16) may be solved in combination with Eq. (12) for the stable equilibrium crack size:

$$c = (16E'd^3W/3p^2)^{1/4}[1 - (1 - hp/W)^{1/2}]^{1/2}. \quad (17)$$

We need to identify an important restriction on Eqs. (12)–(17) developed above. It is implicit in the statement of these relations that the central particle remains in contact with the crack walls, i.e., $u_0 = h$. If the internal pressure p is increased to some critical level, the crack-wall center displacement may indeed exceed this condition, i.e., $u_0 > h$, corresponding to "lift-off". At lift-off, the lenticular crack is supported only by the pressure p, and the center force diminishes to $P = 0$. The formulation then reverts to that of Eqs. (6)–(11). The lift-off pressure may be determined by the requirement that c in Eq. (17) remains real, i.e., $p^* = W/h$. [Strictly, a negative P is physically allowable. That would correspond to total adherence between particle and crack walls ("sticky particle") at high internal gas pressures. In keeping with experimental observations (Sec. III. A) that the crack walls are readily separated on reopening the interface, we exclude this possibility in the present study.]

D. Ideal gas law relations

In our experimental configuration (Sec. III), the pressurized cracks are subject to a constraint; the number of gas molecules N trapped in the crack cavity remains constant after the formation of the interface. We suppose the internal atmosphere satisfies the ideal gas law so that, at a given absolute temperature T, the internal gas pressure p_i varies inversely with the crack volume V. Then Eq. (6) becomes

$$p = NkT/V - p_e, \quad (18)$$

with k Boltzmann's constant.

The volume relation Eq. (9) or (14) may be combined with Eq. (18) to determine the functional dependence $p(c, N, p_e)$ for partially and fully gas-pressurized cracks, and thence substituted into the appropriate fracture mechanics relation Eq. (10) or (16) to determine $G(c, N, p_e)$. For conditions in which N and p_e are held constant during crack extension, it is then tedious but straightforward to show that $\partial G/\partial c < 0$ in both the partially and fully pressurized configurations. The pressure difference p across the crack walls can also be manipulated by varying the external gas pressure p_e.

III. MEASUREMENT OF LENTICULAR-CRACK PROFILES IN MICA

A. Preparation of lenticular cracks in mica

Preparation of the specimens follows prescriptions outlined in previous papers.[8,9,14] A thin sheet of surface dimensions 50 × 50 mm and thickness ≈50 μm was cleaved from bulk muscovite mica. Such sheets were then cut into two halves perpendicular to their cleavage plane. Each pair of halves, after mutual rotation of ≈45° about a common surface normal, was allowed to come into adhesive contact so as to form a "healed-misoriented" interface. Several lenticular cracks were

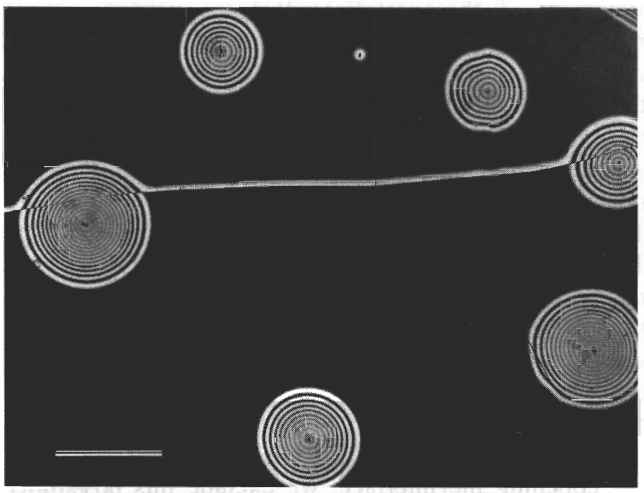

FIG. 2. Micrograph of a portion of a healed adhesion interface in mica after cleavage and mutual rotation of the two specimen halves. Specimen shows several lenticular cracks. Fizeau fringes indicate crack-opening contours. (Line joining cracks at left and right is spurious cleavage step.) Marker indicates 1 mm.

observed at the resealed interfaces of these specimens. Figure 2 is an example. Most of the cracks were found to contain a central particle, most often a microscopic edge flake produced by the specimen preparation. Occasional cracks were found with no such noticeable central particle at all.

After formation, the healed interfaces were allowed to sit for several days, to allow the system to equilibrate. It has been shown[9] that such cracks will expand or contract in delayed response to any substantive increase or decrease in external humidity. Our observations were accordingly made in an ambient laboratory atmosphere of relative humidity ≈40–60%. Previous comparative experiments on open (double-cantilever beam) crack configurations in mica[12–14] indicate an interface energy $W \approx 150 \pm 40\ \mathrm{mJ \cdot m^{-2}}$ at relative humidity 50% for equilibrium cracks formed under such conditions. We take $150\ \mathrm{mJ \cdot m^{-2}}$ as a constant reference value for our later analyses.

Cracks such as those in Fig. 2 could be opened up and re-formed repeatedly by slowly inserting and withdrawing a sharp blade along the healed interface.[13]

B. Crack profile observations

Crack profiles were observed using an inverted microscope with a monochromatic light source.[8] Interference of the light reflected from the opposite crack walls produces a set of concentric two-beam Fizeau fringes. The crack-wall separation at the center of a dark fringe is given by

$$2u(r) = m\lambda/2, \tag{19}$$

where m is the fringe order for constructive interference, and λ is the wavelength ($\lambda = 0.55\ \mu$m, green light). Hence the profile can be constructed by measuring the positions of the interference fringes. We estimate the uncertainty of locating the center of each fringe as ≈0.1 fringe spacing, but omit error bars from our plots below (Sec. IV. B) to avoid data overlap.

Typical internal lenticular cracks are shown in Figs. 3(a) and 4(a). Note that the innermost and outermost fringes are comparatively wider than the intermediate rings, reflecting the boundary condition $du/dr = 0$ at $r = 0$ and $r = c$. The dimensions c and u_0 for each crack can be found by extrapolation of the appropriate displacement relation $u(r)$ in Sec. II to these zero-slope limits.

C. External pressure variations

An experiment was run on the cracks in Figs. 3(a) and 4(a) ($p_e = 1$ atm $= 0.10$ MPa) to investigate the

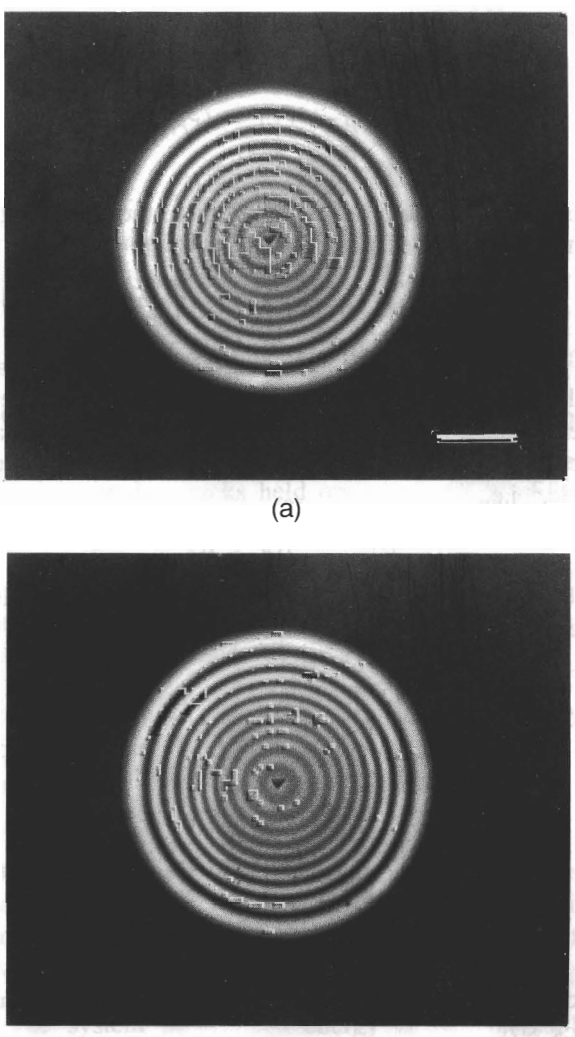

(a)

(b)

FIG. 3. Test crack 1 at healed-misoriented mica interface; external pressure (a) $p_e = 0.10$ MPa and (b) $p_e = 0$. The crack radius increases as p_e diminishes, but the number of fringes remains the same. Marker indicates 250 μm.

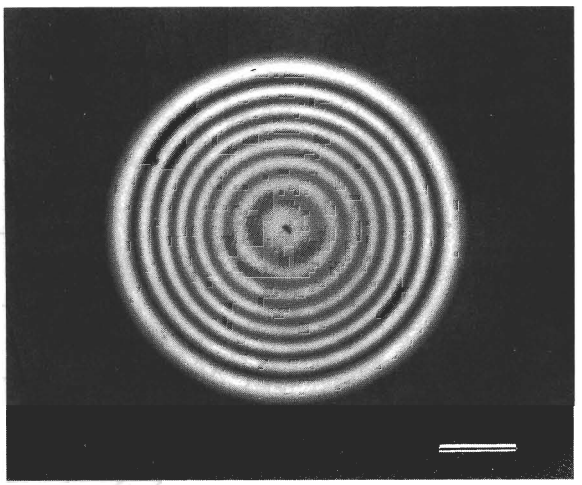

(a)

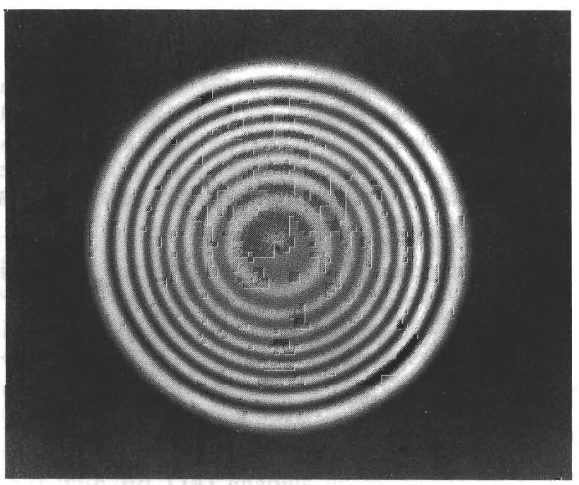

(b)

FIG. 4. Test crack 2 at healed-misoriented mica interface; external pressure (a) $p_e = 0.10$ MPa and (b) $p_e = 0$. Again, the crack radius increases as p_e diminishes, but the number of fringes now also increases by one. Marker indicates 250 μm.

effect of external pressure p_e on the crack profile. The mica specimen was placed inside a sealed chamber with a lead-through to a mechanical vacuum pump. Figures 3(b) and 4(b) show the resultant fringe patterns immediately after evacuation of the chamber. The effect is reversible; i.e., the patterns restore to those in Figs. 3(a) and 4(a) after release of the vacuum.

IV. ANALYSIS OF CRACK PROFILE DATA

A. Qualitative observations of pressurized cracks

In this subsection we describe some qualitative experiments to demonstrate the competitive influence of center-particle support and excess internal gas pressure on the lenticular crack profiles.

First, we draw some immediate conclusions by noting that the number of fringes in cracks of very nearly equal size is not always the same, even in cases where the cracks appear at first sight to be particle supported. Given that the fracture energy W is invariant, we see from Eq. (5) that cracks at constant c in the same specimen imply a constant value of center-point displacement h. Yet the crack in Fig. 3(a) contains two more fringes than that in Fig. 4(a), even though c for the latter crack is slightly larger. The implication is that even if both cracks are indeed particle-supported, an additional net crack-opening force from the internal gas must exist in the larger one. This in turn points to a buildup of internal pressure during the initial recontact adhesion as the mica sheets collapse onto occluded pockets of atmospheric gases.

Consider now the responses of the same cracks at reduced external pressure p_e in Figs. 3(b) and 4(b). In each case the crack size is expanded by the pressure reduction. Notwithstanding such expansion, the crack in Fig. 3(b) shows no measurable change in the number of fringes relative to Fig. 3(a). We may tentatively conclude that this crack remains essentially particle-supported. On the other hand, the crack in Fig. 4(b) shows an extra fringe relative to Fig. 4(a). In this case the subsequent drop in p_e is apparently sufficient to augment any preexisting internal pressure, effecting "lift-off".

Another experiment provides further support of a residual pressure difference at the lenticular cracks. Figure 5 shows the interaction of one such lenticular crack, in a different specimen, with a second, straight-fronted, blade-driven crack.[8] The sequence in Fig. 5 shows (a) slight mutual repulsion on first approach (initial blade insertion), (b) strong repulsion just before coalescence (further blade insertion), and (c) after coalescence (not shown), re-formation of the lenticular crack after withdrawal (blade retraction). The crack retraction in (c) attests to the well-documented atomic smoothness of the cleavage process in mica.[8,11] In many instances in our experiment the crack recovered its initial configuration.[8] However, the crack radius in Fig. 5 is clearly less after the coalescence; the number of interference fringes is reduced from six to five. Note also in Fig. 5(b) that the initial axisymmetry of the crack is severely distorted, and that the trapped particle is now located at the fifth fringe on the near side rather than at the sixth central fringe. This implies that the particle was never in contact with the crack walls in the immediate postformation state; i.e., the cavity was fully gas-pressurized. Presumably the particle is immobile, for otherwise the repulsed lenticular crack would simply have translated with the advancing straight crack. Coalescence appears to have released the internal gas pressure, effectively allowing the internal and external pressures to equilibrate and the crack to re-form with a central-opening displacement equal to the particle diameter. Further passes of the

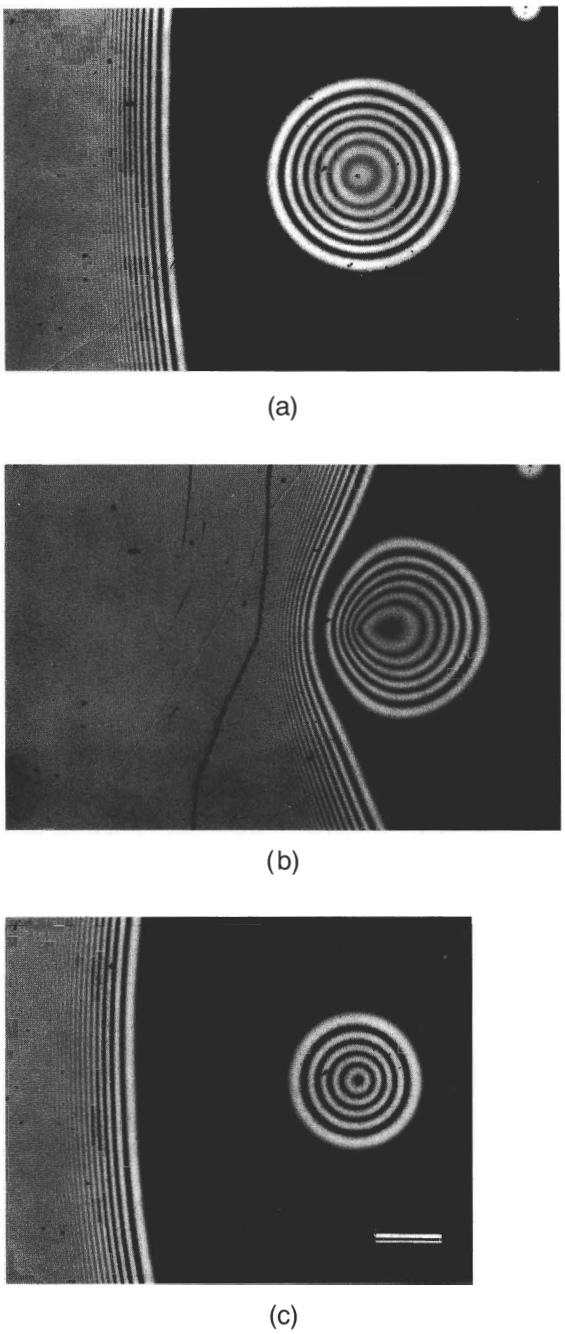

FIG. 5. Lenticular crack and wedge-driven straight-fronted crack along healed mica interface: (a) wedge stationary, cracks noninteractive; (b) wedge advance, cracks in mutual repulsion immediately before coalescence; (c) wedge withdrawal, cracks after coalescence (not shown) and re-formation. Marker indicates 100 μm.

straight crack in Fig. 5 had no further effect on the configuration.

Occasional small cracks were observed to translate with the advancing wedge. Such cracks invariably appeared to be free of internal particles, and could be eliminated by advancing the wedge until the crack perimeters intersected a specimen edge.

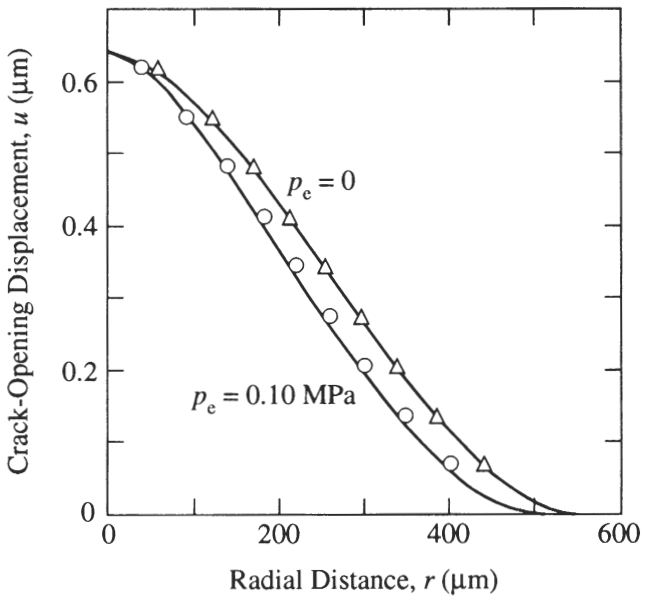

FIG. 6. Profiles of lenticular crack in Fig. 3. Points are measured data, curves are theoretical fits. Crack is particle-supported at both $p_e = 0.10$ MPa (lower curve) and $p_e = 0$ (upper curve).

B. Quantitative measurements of crack profiles

Crack-opening displacements evaluated from Figs. 3–5 using Eq. (19) are plotted as the data points in Figs. 6–8. Curve fitting to these data is done by adjusting parameters in the appropriate $u(r)$ profile equations in Sec. II, consistent with an invariant $W = 150\ \mathrm{J \cdot m^{-2}}$ at $T = 300$ K.

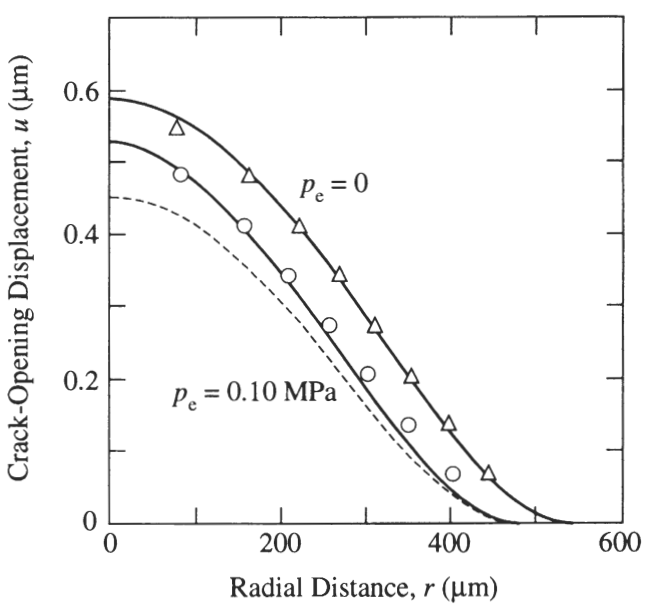

FIG. 7. Profiles of lenticular crack in Fig. 4. Points are measured data, solid curves are theoretical fits. (Dashed curve is projected fit to lower data set assuming crack always remains in "lift-off" condition. See text.) Crack is particle-supported at $p_e = 0.10$ MPa (lower curve), but is in lift-off configuration at $p_e = 0$ (upper curve).

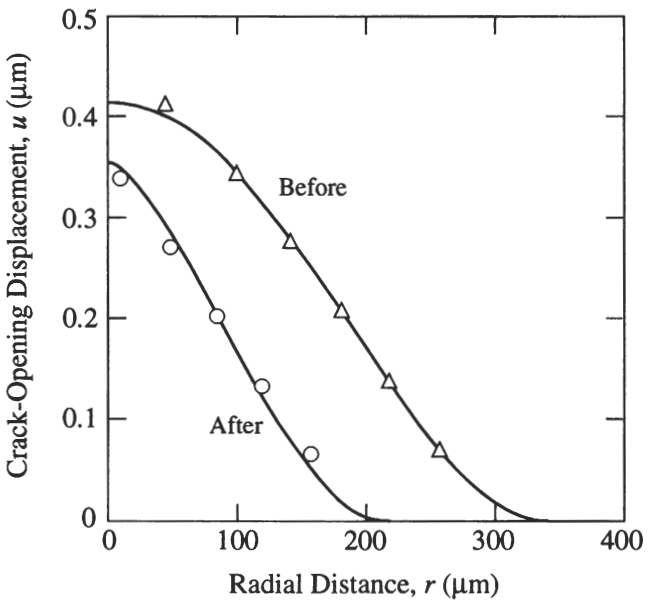

FIG. 8. Profiles of lenticular crack in Fig. 5. Points are measured data, curves are theoretical fits. Upper set corresponds to crack before coalescence with wedge-driven straight crack, lower set after coalescence. Coalescence event releases excess internal gas pressure.

Consider the crack in Fig. 3. Since the number of fringes remains the same in Figs. 3(a) and 3(b), we presume the crack remains particle-supported before and after the reduction in external pressure p_e. To allow for the possibility of a pre-existing pressure difference p in Fig. 3(a), we use $u(r)$ in Eq. (13) as a general profile relation. Examine first the simpler case of zero external pressure in Fig. 3(b). Combining Eq. (18) at $p_e = 0$ with Eq. (14) enables us to eliminate p from Eq. (13), so that $u(r)$ is uniquely determined by just three parameters, h, c, and N. Best fitting the data set for $p_e = 0$ in Fig. 6 yields $h = 0.639$ μm, $c = 559$ μm, and $N = 16.6 \times 10^{12}$ molecules. The profile corresponding to this parameter fit is shown as the upper solid curve in Fig. 6. Now we may *predict* the profile for $p_e = 0.10$ MPa (1 atm) in Fig. 3(a), keeping h and N unchanged and simply determining a new best-fit value for the crack size, $c = 519$ μm. This prediction is shown as the lower solid curve in Fig. 6. This lower curve is consistent with the data set at normal atmospheric external pressure, to within an uncertainty of ± 0.1 fringe spacing (Sec. III. B). With this calibration, we may revert to Eqs. (14) and (18) to estimate a pre-existing excess pressure $p = 0.14$ MPa for the crack in Fig. 3(a).

Now consider Fig. 4. Clearly, the lift-off condition has been exceeded in Fig. 4(b), so $u(r)$ is given by Eq. (7) for fully gas-pressurized cracks. Combining Eq. (18) at $p_e = 0$ with Eq. (9) to solve for p and inserting back into Eq. (7), we find this time that $u(r)$ is uniquely determined by just two parameters, c and N. Best fitting the data set for $p_e = 0$ yields $c = 639$ μm and $N = 30.9 \times 10^{12}$ molecules. The corresponding profile is shown as the upper solid curve in Fig. 7. Now if we use these best-fit values to predict the profile for the crack in Fig. 4(a) using Eq. (7) at $p_e = 0.10$ MPa, we obtain the dashed curve in Fig. 7. This predicted curve falls well below the lower data set, so we conclude that the crack-opening displacement must be constrained by the internal particle. Accordingly, we recompute the displacement profile by once more invoking Eq. (13), at the same N but with adjustments $h = 0.530$ μm and $c = 569$ μm. The resulting lower solid curve in Fig. 7 provides a more satisfactory fit to the data. Again, we may evaluate a pre-existing excess pressure, $p = 0.28$ MPa, for the crack in Fig. 4(a) ($p_e = 0.10$ MPa), i.e., significantly higher than for the crack in Fig. 3(a).

Finally, we plot the profiles for the crack in Figs. 5(a) and 5(c). Again, it is clear that the crack is in full gas-pressure support in Fig. 5(a), and full particle support at $p = 0$ in Fig. 5(c). Our fitting procedure is the same as in the preceding paragraph, except that we now no longer constrain N to have the same value before and after coalescence. The fits shown in Fig. 8 correspond to the following adjustments: $c = 336$ μm and $N = 10.9 \times 10^{12}$ molecules in (a); $h = 0.357$ μm, $c = 220$ μm, and $N = 0.66 \times 10^{12}$ molecules in (c). The number of gas molecules within the crack cavity is reduced by over an order of magnitude by the coalescence event.

V. DISCUSSION

We have considered the equilibrium states of lenticular cracks in the thin interlayer geometry of Fig. 1 under the constraints of fixed particle size h and number of molecules N. It is readily shown that under these constraints the equilibria are inherently *stable*, even when the cracks are fully gas-pressurized. Recall that the condition for a crack to be *stable* is that $dG/dc < 0$; and conversely, to be *unstable*, $dG/dc > 0$.[15] For our cracks at fixed h and N, G is always a diminishing function of crack size c. The purely particle-supported crack ($p = 0$) is especially stable. From Eqs. (2) and (4), we have $G(c) = 4E'd^3h^2/3c^4$, i.e., inverse fourth power dependence on c at h constant. Not so strongly dependent on c, but stable nonetheless, is the fully gas-pressurized crack ($u_0 > h$), as we may illustrate by considering the simplest external pressure condition, $p_e = 0$. From Eqs. (9), (10), and (18) we obtain $G(c) = 3NkT/2\pi c^2$, i.e., inverse square dependence on c at N constant. It is straightforward (if tedious) to demonstrate that cracks in combined particle and pressure support lie intermediate between these two stability extremes.

Note that by invoking the equilibrium condition, $G = W$, we can express the crack-opening displace-

ment and crack radius in terms of W. For the fully particle-supported crack, we have $u_0 = h$ [Eq. (2)] and $c = (4E'd^3h^2/3W)^{1/4}$ (previous paragraph). Then u_0 is independent of E' and d, but c is not. For the fully gas-pressurized crack at $p_e = 0$, the corresponding relations are $u_0 = 27p(NkT)^2/16E'd^3W$ [Eqs. (8), (9), and (18)] and $c = (3NkT/2\pi W)^{1/2}$ [Eqs. (9)–(11) and (18)]. Now it is u_0 that is dependent on E' and d, and c that is not. Accordingly, if one were able to reduce the material modulus or specimen thickness, the crack in particle support ($u_0 = h$ = constant) would contract in radius but remain fixed in center opening, whereas a crack in internal gas support (N, T constant) would remain fixed in radius but bulge outward at its center.

We have specifically considered the *double*-layer thin-plate system in Fig. 1. However, our analysis may be logically extended to the analogous *single*-layer system of a thin coating on a thick (semi-infinite) substrate. Then for simple mode I loading, the mechanical energy of an interfacial crack derives from the deflection of one elastic plate instead of two, corresponding to a reduction of two in the crack-driving force; i.e., $G(c) = 3NkT/4\pi c^2$ for a fully gas-pressurized crack. Strictly, conversion to the single-layer geometry destroys the specimen symmetry about the crack plane, leading to the superposition of a mode II component in the loading,[16] with consequent augmentation of the net G. However, this will not alter the fundamental crack-size dependence of G, so the crack remains stable.

Another crack geometry of common interest is the case of a fully embedded crack in an infinite medium. The basic fracture mechanics for a gas-pressurized penny crack in a bulk solid are included in the Appendix. Although the thin-plate theory is no longer valid, $G(c) = 3NkT/4\pi c^2$, i.e., the same (mode I) result as above for a thin coating on a semi-infinite substrate. Therefore, at constant N, the system is yet again stable.

An interesting variant of the coating/substrate configuration in relation to crack stability is the use of the so-called "blister test" for determining interface properties.[17] Gas is pumped into the interface under pressure control. Under these special conditions we have $G(c) \propto p^2c^4$ from Eq. (10), and the equilibrium at constant p is consequently *unstable*. On perturbing the equilibrium, the coating fails catastrophically, so the critical pressure provides a measure of the interface strength.

Instances also exist where N may be increased within the crack cavity *without* compromising the stability. We cite two cases here:

(i) Sheets of virgin (phlogopite) mica with lenticular flaws similar to those observed in the present study, but on a smaller scale, are beam heated in a transmission electron microscope.[5] The flaws contain liquid water, which is unable to diffuse out along the interface to the external atmosphere[9]; the virgin interface at the crack plane, in contrast to the healed-misoriented interface in our mica specimens, is not in a state of lattice-plane dilation. On heating above the boiling point, the occluded water evaporates, dramatically increasing the number of molecules N in the gaseous state. The result is a rapid expansion of the crack radius. This expansion is nevertheless stable and is usually reversible on reducing the beam intensity. In extreme cases, those where the quantity of internally trapped water is unusually large, the expansion extends to the edge of the specimen, thereby rupturing the sheet irreversibly.[5]

(ii) Crystals of lithium fluoride containing submicroscopic inclusion-type defects are irradiated with a high-power laser pulse.[7] The inclusions preferentially absorb the laser radiation, and evaporate virtually instantaneously, filling the cavity with an expanding gas. This causes sudden penny-crack growth along favored {001} cleavage planes. In lithium fluoride the cleavage is far removed from the atomic smoothness of mica, and copious wedging fracture debris remain to restrain the cracks from closing up and healing.[7]

The crack evolution in these two examples may be depicted graphically as transitions between stable branches on a $G(c)$ diagram, as in Fig. 9. A, B, and C are Griffith–Irwin equilibrium states, $G = W$. Suppose the crack is initially in particle support ($G \propto h^2/c^4$), state A. On heating or irradiating the cavity, the gases expand, lifting the walls off the particle ($G \propto N/c^2$) and enlarging the crack radius, state B. If the crack is reversible [as in example (i) above], it reverts to state A. If debris become wedged between the newly expanded

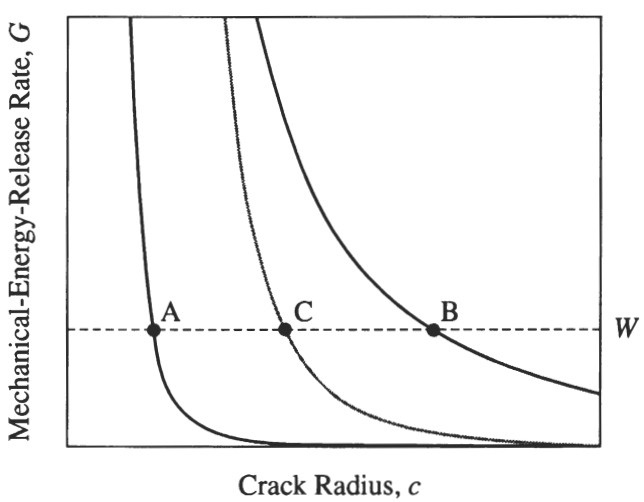

FIG. 9. Plot of $G(c)$ for lenticular flaw, showing equilibrium configurations A, B, and C at $G = W$. State A corresponds to the initial particle-supported crack; state B is lifted-off crack after an abrupt expansion of internal gas; state C is relaxed particle-supported crack after recondensation of released gas. Note all states are stable ($dG/dc < 0$).

walls [as in example (ii) above], the crack is held open in enhanced particle support ($G \propto h'^2/c^4, h' > h$), state C.

Internally pressurized cracks simulate the conditions that exist in many real flaws in brittle solids, including those formed in ceramics as a result of the processing chemistry and those formed by subsequent mechanical, thermal, or radiation treatments. Such pressure provides an extra, residual crack-driving force, which can augment any applied loading and lead to premature failure. Such concerns are particularly relevant to the fracture of coatings on substrates, to subsurface regions in contact (especially sliding) loads, and to materials in severe radiation (e.g., reactor) environments.

ACKNOWLEDGMENTS

The authors are grateful to D.T. Smith for discussions. Funding for this project was provided by the United States Office of Naval Research.

REFERENCES

1. A.A. Griffith, Philos. Trans. R. Soc. London **A221**, 163–198 (1920).
2. B.R. Lawn, *Fracture of Brittle Solids* (Cambridge University Press, Cambridge, 2nd ed., in press).
3. A.G. Evans and J.W. Hutchinson, Int. J. Solids Struct. **20** (5), 455–466 (1984).
4. M.V. Swain, Wear **35**, 185–189 (1975).
5. L. Cartz and B. Tooper, J. Appl. Phys. **36** (9), 2783–2787 (1965).
6. B.R. Lawn and E.R. Fuller, J. Mater. Sci. **19**, 4061–4067 (1984).
7. Z-Y. Wang, M.P. Harmer, and Y.T. Chou, Mater. Lett. **7** (5–6), 224–228 (1988).
8. K-T. Wan, B.R. Lawn, and R.G. Horn, J. Mater. Res. **7**, 1584–1588 (1992).
9. R.G. Horn, K-T. Wan, S. Courmont, and B.R. Lawn, J. Colloid and Interf. Sci. (in press).
10. W.C. Young, *Roark's Formulas for Stress and Strain* (McGraw-Hill, New York, 1989).
11. A.I. Bailey and S.M. Kay, Proc. R. Soc. London **A301** (1464), 47–56 (1967).
12. K-T. Wan and B.R. Lawn, Acta Metall. **38** (11), 2073–2083 (1990).
13. K-T. Wan, N. Aimard, S. Lathabai, R.G. Horn, and B.R. Lawn, J. Mater. Res. **5**, 172–182 (1990).
14. K-T. Wan, D.T. Smith, and B.R. Lawn, J. Am. Ceram. Soc. **75** (3), 667–676 (1992).
15. Y-W. Mai and B.R. Lawn, Ann. Rev. Mater. Sci. **16**, 415–439 (1986).
16. J.W. Hutchinson and Z. Suo, Adv. Appl. Mech. **29**, 64 (1991).
17. G.P. Anderson, S.J. Bennett, and K.L. DeVries, *Analysis and Testing of Adhesive Bonds* (Academic Press, New York, 1977).
18. I.N. Sneddon and M. Lowengrubb, *Crack Problems in the Classical Theory of Elasticity* (John Wiley, New York, 1969).

APPENDIX: GAS-PRESSURIZED INTERNAL LENTICULAR CRACKS IN AN INFINITE ELASTIC MEDIUM

Consider a penny-like crack of radius c embedded in an infinite elastic medium of modulus E' with internal gas pressure p. The crack profile is the classical ellipsoid[18]

$$u(r) = (4p/\pi E')(c^2 - r^2)^{1/2}. \tag{A1}$$

The volume of the crack void is

$$V = 16pc^3/3E'. \tag{A2}$$

Combining the Griffith–Irwin mechanical-energy-release rate with Eq. (18) at $p_e = 0$ yields[2]

$$G = 4p^2c/\pi E' = 3N\mathrm{k}T/4\pi c^2. \tag{A3}$$